Pellet Printing for Soft Devices

*Yijia Wu, Ju-Hung Chen, Ariana Olivares, Katherine Kostak, Stefan Pedicone, Savita Kendre, and Markus P. Nemitz**

Y. Wu, J. Chen, A. Olivares, K. Kostak, S. Pedicone, Dr. S. Kendre, Prof. M. P. Nemitz

Department of Mechanical Engineering, Tufts University, Medford, MA 02155, USA

Email Address: markus.nemitz@tufts.edu

1 Material preparation

All raw compliant materials used in this study were commercially sourced (**Table SS1**). To prevent moisture-induced defects such as cavity formation from water evaporation at the print nozzle, all filaments and pellets were pre-dried in a filament dryer (Sunlu S4) at 60 °C for 6 hours and subsequently stored in a dry cabinet (Manncorp Ultra-Dry 790V) maintained below 5% relative humidity (RH) until use.

Table S1: The materials we used in this study, with corresponding shore hardness and manufacturers.

Material Type	**Material**	**Shore Hardness**	**Manufacturer**
TPE pellets	TF1STL	6A	KRAIBURG TPE
	TF2STL	10A	KRAIBURG TPE
	TF2ATL	22A	KRAIBURG TPE
	TF4ATL	40A	KRAIBURG TPE
	TF5ATL	50A	KRAIBURG TPE
TPE filaments	Filaflex 60A	63A	Recreus
	Filaflex 70A	70A	Recreus
	NinjaFlex Edge	83A	NinjaTek
Silicone	Ecoflex 00-50	00-50	Smooth-On
	Dragon Skin 10 Fast	10A	Smooth-On
	Dragon Skin 20	20A	Smooth-On
	Dragon Skin 30	30A	Smooth-On

2 Material selection

There are three additional sets of TPE pellets that were tested but ultimately excluded from this study due to various limitations.

The first set comprised TPS pellets from Yangzhou Baiyu (ranging from 00-30 to 50A). While these materials could be printed into functional structures, including airtight PneuNet actuators, their surfaces were excessively tacky, leading to inconsistent extrusion and severe stringing that compromised print reliability.

The second set included TPU pellets from Recreus, corresponding to the material used in their Filaflex 60A filament. Likely optimized for filament-based FFF printing, these pellets were formulated to melt rapidly. Consequently, even at relatively low temperatures (160 °C), the material exhibited excessively low viscosity inside the barrel, resulting in uncontrolled flow.

The third set consisted of very soft TPS pellets from KRAIBURG TPE (00-51 and 00-32 Shore hardness). Although simple, small structures could be printed, the resulting parts exhibited poor surface quality and were too fragile to support more complex or airtight geometries.

We conclude that soft materials suitable for FGF printing should exhibit good thermal stability to withstand extended heating within the barrel (on the order of minutes), low surface tackiness to minimize sticking to the walls or to each other, and an appropriate melting range combined with shear-thinning behavior to enable effective flow control and reduce stringing.

3 Printer modifications

The printer was systematically modified to improve reliability and performance when printing soft TPS pellets. The key modifications are summarized below:

- A higher-speed cooling fan was installed to minimize heat creep and prevent premature softening of pellets (**Figure SS1**).
- The pellet hopper was redesigned with a steeper wall angle to promote consistent gravitational flow.
- Internal surfaces of the hopper were coated with polytetrafluoroethylene (PTFE) spray to reduce friction and mitigate pellet bridging.
- Polypropylene tape was applied to the print bed to improve first-layer adhesion and prevent warping.
- A time-of-flight sensor was integrated to monitor pellet levels in the hopper and prevent extrusion issues due to low material volume.

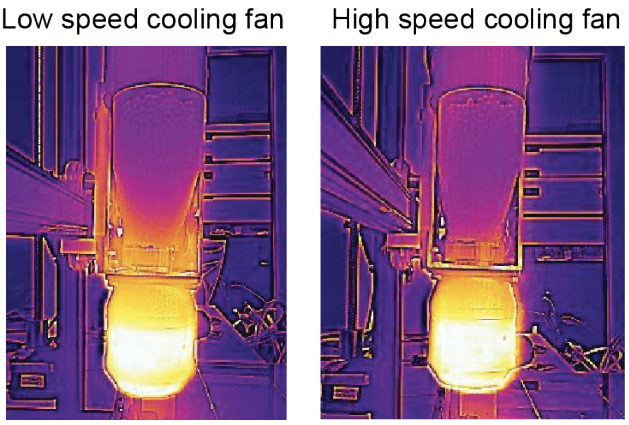

Figure S1: **Heat creep prevention.** Thermal image of the print head before and after installing a high-speed cooling fan.

4 Print parameters

For each material, identical print parameters were used to fabricate both the tensile test specimens and the PneuNet actuators, ensuring that the tensile data could be directly applied to numerical simulations of the actuators (**Table S2, S3**). A fixed print speed of 30 mm/s was selected for all TPS pellets to maintain consistent print quality across materials. However, stiffer materials demonstrated compatibility with higher print speeds without compromising airtightness. Accordingly, an additional set of optimized print parameters for high-speed, airtight printing with stiffer materials is also provided (**Table S4**).

Table S2: General FGF and FDM printing parameters. *Refer to **Tables S3 and S4** for detailed extrusion parameters for pellets of different Shore hardness.

Parameter	**FGF**	**FDM (60A, 70A)**
Nozzle size (mm)	0.5	0.5
Layer height (mm)	0.2	0.2 (test bars)/ 0.1 (airtight parts)
Print speed (mm/s)	30	10
Infill overlap (mm)	0.2	0.25
Retraction distance (mm)	0.8	0
Extrusion multiplier	*	1.3

Table S3: FGF print parameters for TPE materials of different Shore hardnesses, used for printing tensile test bars and PneuNets.

Parameter	**6A**	**10A**	**22A**	**40A**	**50A**
Print speed (mm/s)	30	30	30	30	30
Nozzle temperature (°C)	215	215	240	240	240
Bed temperature (°C)	60	60	30	30	30
Initial layer flow (%)	160	160	120	150	200
Overall flow (%)	160	160	180	320	500
Wall flow (%)	180	180	200	420	550

Table S4: High speed FGF print parameters for 22A to 50A TPE materials.

Parameter	**22A**	**40A**	**50A**
Print speed (mm/s)	40	50	50
Nozzle temperature (°C)	240	240	240
Bed temperature (°C)	30	30	30
Initial layer flow (%)	100	150	150
Overall flow (%)	160	250	350
Wall flow (%)	180	300	380

5 FGF print parameter tuning

Because the TPS pellets were not originally formulated for 3D printing, no official print parameters are provided by the manufacturer. Instead, recommended injection molding parameters were used as a starting point. These guidelines specify cylinder temperatures for a standard 3-zone polyolefin screw, whereas the print head used in this study features a single heating zone. Consequently, the recommended final melt temperature was selected as the initial nozzle temperature, and the specified maximum temperature was adopted as the upper limit.

Print parameter tuning was conducted in two main stages. The first stage focused on establishing basic printability, defined as consistent material extrusion at practical speeds with sufficient bonding between adjacent lines and layers. Nozzle and bed temperatures were the primary variables at this stage and were typically adjusted at reduced print speeds to increase reliability, with flow rate calibrated accordingly. Calibration blocks and tensile test specimens served as evaluation structures during this phase. The second stage aimed to achieve airtight printing suitable for pneumatic devices. This required optimizing the interplay among print speed, flow rate, and temperature to ensure consistent deposition, complete layer fusion without internal voids, and minimal oozing. The primary objective was to maximize print speed without compromising airtightness. The PneuNet actuator served as the benchmark geometry for this optimization phase.

5.1 Flow rate conversion

To ensure compatibility with existing slicer software and firmware designed for filament-based systems, it is necessary to convert the desired volumetric flow rate in FGF printing into an equivalent screw rotation speed. The following derivation describes this conversion process. The desired volumetric flow rate, Q_{desired}, can be calculated as

$$Q_{\text{desired}} = dhv \tag{1}$$

where v is the print speed, d is the nozzle diameter, and h is the layer height. When the flow factor f is not set to 100%, the flow rate is adjusted to

$$Q_{\text{adjusted}} = fQ_{\text{desired}} \tag{2}$$

The adjusted flow rate Q_{adjusted} is then used to determine the required extrusion motor rotation speed.

Since most slicers and 3D printer firmware are designed for FFF printers, the conversion from flow rate to motor speed is based on

$$Q_{\text{adjusted}} = A_f v_f = \pi \frac{D^2}{4} v_f, \tag{3}$$

where A_f is the cross-sectional area of the filament, v_f is the filament feed rate driven by the extrusion motor, and D is the filament diameter.

The rotation speed ω of the extrusion screw in an FGF printer can then be linked to the equivalent filament feed rate v_f using the rotation distance d_r as

$$\omega = \frac{v_f}{d_r} \tag{4}$$

Here, d_r corresponds to the parameter `rotation_distance`, which can be set in Klipper firmware. In this study, the default value of 7.6190 (as provided in the Ender 3 printer configuration file) was used.

5.2 Extrusion test

To find a balance among print speed, flow rate, and temperature, an extrusion test was designed to characterize both the achievable volumetric flow rate and oozing behavior. For each test, the nozzle was preheated to the target temperature, after which the extrusion screw was rotated at a set speed for a chosen duration sufficient to collect a measurable amount of extruded material. Using the measured mass m, extrusion time t, and material

density ρ, the volumetric flow rate was calculated as

$$Q = \frac{m}{\rho t} \tag{5}$$

Immediately after extrusion stopped, the nozzle was manually wiped and a small retraction was applied. The subsequent oozing process was recorded on video, and the oozed filament length was later measured over time.

Experimental results indicated that both volumetric flow rate and oozed length increased with higher screw rotation speeds. A threshold oozing criterion was then selected to determine an acceptable rotation speed. For example, using 22A pellets at 240 °C, a limit of 5 mm oozing within 5 seconds was chosen, corresponding to a rotation speed of 16 rpm. Once the rotation speed was determined, the corresponding volumetric flow rate could be used to calculate the appropriate print speed using the relationships derived in the previous section.

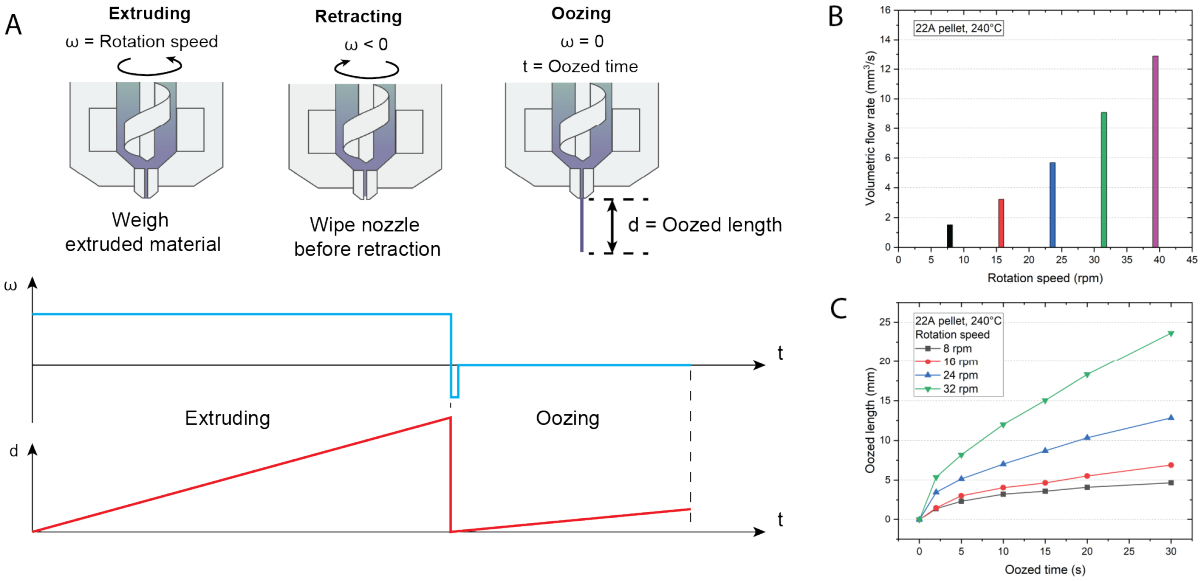

Figure S2: **Extrusion test process and result.** (A) Schematic illustration of the extrusion test process. (B) Volumetric flow rate versus screw rotation speed, showing the upper limit before excessive oozing occurs. (C) Oozed length as a function of oozed time at different screw rotation speeds for 22A pellets at 240 °C.

6 Additional material characterization

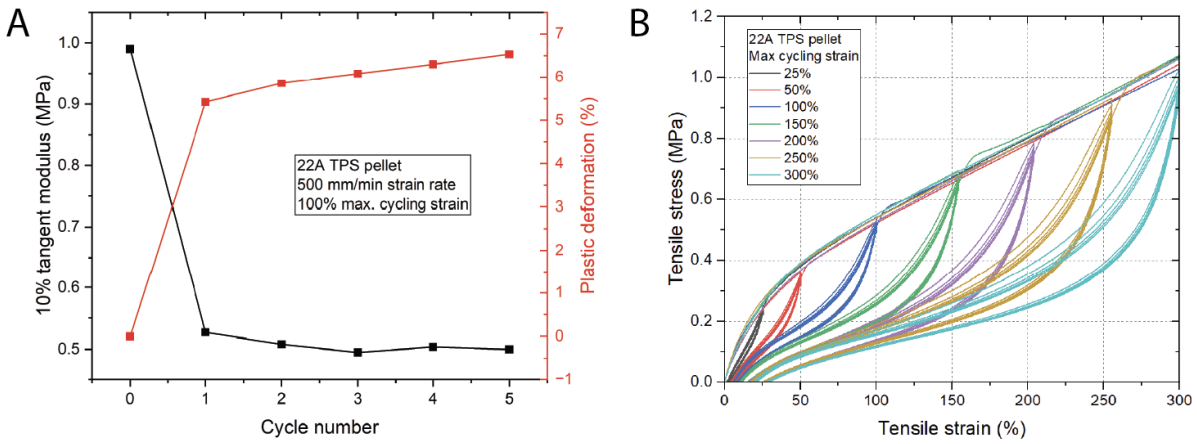

Figure S3: **Cyclic tensile behavior of 22A TPS pellets.** (A) Evolution of 10% tangent modulus and plastic deformation over five loading–unloading cycles at 100% maximum strain, illustrating Mullins effect and stabilization after the first cycle. (B) True stress–strain curves for different maximum cyclic strains, showing progressive plastic deformation and stiffness reduction with higher strains.

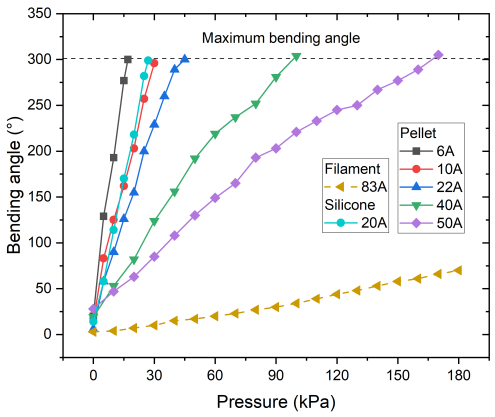

Figure S4: **Pressure–bending response of actuators fabricated from various materials.** Bending angle versus input pressure for actuators printed with TPS pellets (6A, 10A, 22A, 40A, 50A), TPU filament (83A), and molded silicone (20A). Softer materials achieve larger bending angles at lower pressures.

7 Hyperelastic model fitting

Uniaxial tensile tests were performed on each TPS pellet according to ASTM D412 standards for vulcanized rubbers and elastomers to characterize their mechanical properties. All specimens sustained strains exceeding 200% and exhibited large deformations comparable to silicone rubbers. Accordingly, the Ogden model was selected as the hyperelastic constitutive model, given its suitability for capturing nonlinear elastic behavior at high strains. The data fitting procedure followed a standard hyperelastic modeling approach [1]. In an N-order Ogden model, the strain energy density W is expressed with three principal stretches $\lambda_j, j = 1, 2, 3$

$$W(\lambda_1, \lambda_2, \lambda_3) = \sum_{p=1}^{N} \frac{\mu_p}{\alpha_p} \left(\lambda_1^{\alpha_p} + \lambda_2^{\alpha_p} + \lambda_3^{\alpha_p} - 3\right) \tag{6}$$

where μ_p and α_p are material parameters. Under the isotropic incompressible material property and uniaxial loading assumption, the principal Cauchy stress σ_{uniax} function can be derived as

$$\sigma_{\text{uniax}} = \sum_{p=1}^{n} 2\mu_p \left[\lambda^{\alpha_p - 1} - \lambda^{-\frac{1}{2}\alpha_p - 1}\right] \tag{7}$$

To estimate the Ogden coefficients (μ_p, α_p), the mean true stress–strain response from five tensile tests was first calculated. The `least_squares` function from `scipy.optimize` in Python was then used to minimize the sum of squared errors between the predicted Cauchy stress (based on the estimated coefficients) and the experimental Cauchy stress. Since the initial coefficient values can influence the optimization outcome, the standard error of the estimate S was used to evaluate the fitting performance. Ten sets of random initial coefficients were tested, and the model with the lowest S value was selected as the final result. Here, y_i denotes the experimental value, $\hat{y}_i$ the predicted value, n the number of data points, and k the number of coefficients.

$$S = \sqrt{\frac{\sum_{i=1}^{n}(y_i - \hat{y}_i)^2}{n - k - 1}} \tag{8}$$

For each material, Ogden models of first-, second-, and third-order were all fitted, and the model yielding the lowest standard error S was selected and reported in **Table SS5** for use in numerical simulations.

Table S5: Fitted Ogden model parameters for materials with different Shore A hardness.

Shore A	μ_1 **(MPa)**	μ_2 **(MPa)**	μ_3 **(MPa)**	α_1	α_2	α_3
6	0.00036	0.04168	–	5.36505	2.27831	–
10	0.00020	0.07418	–	6.07880	2.73905	–
22	0.17570	-0.02606	-0.12322	3.79427	-9.71010	4.32167
40	-0.18264	-0.17852	0.41687	-12.42437	6.22649	2.16209
50	-0.29832	-0.30330	0.65090	6.43886	-12.85631	2.02424

8 Comparison of 3D printing techniques for soft devices

Table S6: Comparison of 3D printing methods for printing soft devices.

Category	FGF	FFF	DIW	SLA/DLP	Inkjet	SLS
Printer cost	Low–Medium	Low	Medium–High	Medium	High	High
Post-processing	Minimal	Minimal	Required (curing)	Required	Required	Required
Multimaterial printing	Yes	Yes	Yes	Limited	Yes	No
Print speed	Medium–Fast	Medium	Slow	Fast	Very high	Medium–Fast
Print resolution	Medium	Medium	Low–Medium	Very high	Very high	High
Structure complexity	Medium	Medium	Medium	High	Very high	High
Layer Adhesion	Poor	Poor	Good	Good	Good	Medium

Table S7: Comparison of the soft materials available for different 3D printing methods.

Category	FGF	FFF	DIW	SLA/DLP	Inkjet	SLS
Representative Materials	TPE (TPS, TPU), EVA pellets	TPU, soft PLA filaments	Silicone, hydrogels, PDMS	UV-curable acrylate-based resins	UV-curable acrylate-based resins	TPE powders
Material cost	Low	Medium	Medium	Medium–High	High	High
Material availability	Broad	Medium	Medium	Limited	Limited	Very limited
Recyclability	High	High	None	None	None	Partially
Minimum Shore hardness	<5A	63A	<5A	40A	32A	45A
Max elongation at break	>1000%	500–700%	>1000%	100–300%	100–300%	100–300%
Elastic recovery	Medium	Medium	Good	Poor	Poor	Medium
Strain softening	Medium–High	Medium	Low	High	High	Medium

References

[1] L. Marechal, P. Balland, L. Lindenroth, F. Petrou, C. Kontovounisios, F. Bello, "Toward a Common Framework and Database of Materials for Soft Robotics", *Soft Robotics* **2021**, *8*, 3 284.